THE JOURNAL OF PHYSICAL CHEMISTRY B
A JOURNAL OF THE AMERICAN CHEMICAL SOCIETY

pubs.acs.org/JPCB

Article

Micro-Solvation of Propofol in Propylene Glycol−Water Binary Mixtures: Molecular Dynamics Simulation Studies

Anupama Sharma, Vishal Kumar, and Sudip Chakraborty*

Cite This: https://doi.org/10.1021/acs.jpcb.3c04932

Read Online

ACCESS | Metrics & More | Article Recommendations

ABSTRACT: The water microstructure around propofol plays a crucial role in controlling their solubility in the binary mixture. The unusual nature of such a water microstructure can influence both translational and reorientational dynamics, as well as the water hydrogen bond network near propofol. We have carried out all-atom molecular dynamics simulations of five different compositions of the propylene glycol (PG)/water binary mixture containing propofol (PFL) molecules to investigate the differential behavior of water microsolvation shells around propofol, which is likely to control the propofol solubility. It is evident from the simulation snapshots for various compositions that the PG at high molecular ratio favors the water cluster and extended chainlike network that percolates within the PG matrix, where the propofol is in the dispersed state. We estimated that the radial distribution function indicates higher ordered water microstructure around propofol for high PG content, as compared to the lower PG content in the PG/water mixture. So, the hydrophilic PG regulates the stability of the water micronetwork around propofol and its solubility in the binary mixture. We observed that the translational and rotational mobility of water belonging to the propofol microsolvation shell is hindered for high PG content and relaxed toward the low PG molecular ratio in the PG/water mixture. It has been noticed that the structural relaxation of the hydrogen bond formed between the propofol and the water molecules present in the propofol microsolvation shell for all five compositions is found to be slower for high PG content and becomes faster on the way to low PG content in the mixture. Simultaneously, we calculated the intermittent residence time correlation function of the water molecules belonging to the microsolvation shell around the propofol for five different compositions and found a faster short time decay followed up with long time components. Again, the origin of such long time decay is primarily from the structural relaxation of the microsolvation shell around the propofol, where the high PG content shows the slower structural relaxation that turns faster as the PG content approaches to the other end of the compositions. So, our studies showed that the slower structural relaxation of the microsolvation shell around propofol for a high PG molecular ratio in the PG/water mixture correlate well with the extensive ordering of the water microstructure and restricted water mobility and facilitates the dissolution process of propofol in the binary mixture.

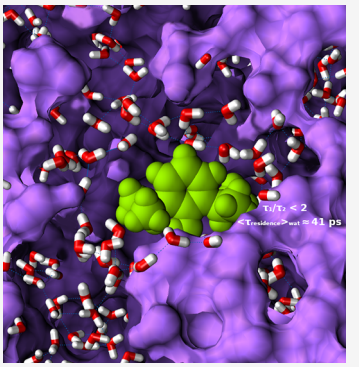

INTRODUCTION

Bioavailability of poorly soluble drugs poses a significant challenge owing to their stability and formulation.[1] Water solubility is one of the key parameters that influence the drugs' ability to dissolve in bodily fluids and being directly absorbed.[2] Hence, improving drug bioavailability has led to constant growth of an array of delivery mechanisms and solution preparation in modern drug development.[1,3,4] In recent years, studies have shown that water molecules present at the interface between the drug and the receptor plays a crucial role in the binding process.[5,6] Additionally, water molecules present in the vicinity of the receptor can also influence the activity of anesthetics both local and general.[7] This underscores the importance of understanding the interactions between anesthetics and water molecules first in order to better understand and improve the efficacy of these drugs. A preferential solvation study of drug molecules in alcohol−water,[8,9] glycol−water cosolvent mixtures,[10−12] and ionic liquid−water cosolvent composition[13,14] has been reported. Several aqueous alcohol mixtures of varying compositions, temperatures and pressures have been studied for industrial importance too.[15−18]

Propofol (2,6-diisopropylphenol) is a general intravenous anesthetic molecule, developed by John Baird Glen in search of safer and effective anesthesia.[19] It is widely used due to its rapid onset and quick recovery.[20] Studies suggest propofol pose its action on presynaptic receptors, it activates $GABA_AR$ function and[21−23] inhibits voltage gated sodium ion channels.[24] It is a phenolic compound with two isopropyl groups ortho to sterically hindered hydroxyl group. Steric

Received: July 21, 2023
Revised: November 1, 2023
Accepted: November 1, 2023

hindrance due to the presence of two alkyl groups obstructs the formation of hydrogen bonds in aqueous media. Thus, propofol is merely soluble in aqueous solution with the octanol/water partition coefficient reported as 6761:1.[25] Emulsion based formulation is available as Diprivan which is composed of soybean oil, glycerol, and purified egg phosphatide for intravenous use in clinic.[26] Though they are found to have minor incidence of postoperative nausea and vomiting, risk associated with long-term uses such as pain on injection, hyperlipidemia, and poor physical stability, bacterial contamination after exposure to air is not uncommon[27−33] Considering the clinical potency, studies persisted in search for safer and efficacious vehicles.[34−36]

Propylene glycol (PG) is an industrially important amphiphilic diol[37−40] It is a viscous liquid with the ability to reduce water crystallization and melting which makes its use in antifreeze solutions.[38,39] The high specific heat capacity of the PG−water mixture gives its potential application in gasifying liquefied natural gas.[37] It is known for its lipid destabilizing role[40] and used as a chemical enhancer in topical formulation to cure skin disorders.[41−43] It has gained interest in cell preservation for its cryoprotectant ability in solutions.[44] It is considered safe for administrative purposes and hence used to dissolve several drug molecules in drug administrative formulation.[45,46] Several experimental investigation for the aqueous propylene−glycol water mixtures have been reported[47−50] However, the understanding of the solution for the prevention of water crystallization was the main principal in the works.[4749] Considering the safety, PG is the most widely used cosolvent in the design and development of liquid medicines.[51] It has been used as a testing solvent model for the solubility of several drug molecules in experiments.[5253] Jiménez et al. studied the effect of PG water mixture concentration on three pharmaceutical salts of varied pH values.[54] The driving mechanism for the solubility of drug meloxicam in water-rich composition was due to disturbed water-structure near the drug and is entropic in nature, while for PG-rich, it is enthalpic due to better solvation.[12] Gao and Olsen studied the extent of drug acetaminophen release in aqueous NaCl solution, suggesting interplay between interaction forces with solvent molecules and with other drugs.[55] Trapani et al. studied the solubility of propofol in 1:1 v/v PG/water binary solution. They found the mixture was able to solubilize 10 mg/mL of propofol with induction time and duration of action comparable to that of Diprivan.[35]

Solubilization of propofol in aqueous solution has been reported in several experimental investigation.[36,56−61] Dwyer et al. studied propofol in the aqueous solutions of Pluronics where increased propofol in solution induces micelle formation and propofol is likely to be solubilized in the core.[56] Cho et al. studied the microemulsion of propofol for intravenous injection formulated using aqueous nonionic surfactants, poloxamers, and polyethylene glycol 660 hydroxystearate. This new formulation was found to cause considerably low histamine release compared to the macroemulsion earlier reported.[57] The nuclear magnetic resonance (NMR) study of propofol in nonionic surfactants reveals higher diffusion coefficient of propofol than that of the surfactant caused by the partitioning of propofol between swollen micelles and the aqueous solution.[58] The vibrational sum frequency generation technique was used to understand the dissociation as well as hydration of propofol at the water interface under different pH conditions.[59] Duration of unresponsiveness to propofol ingestion combined with the remifentanil-fentanyl anesthetic has been reported using combined pharmacokinetic pharmacodynamic models.[60] Drug delivery potency of cyclodextrin molecules with propofol has been tested and found to improve its pharmacokinetic and pharmacodynamic properties at the blood brain barrier.[36] Mass-resolved excitation spectroscopy suggests the formation of a homodimer and its single hydrogen bond bridge propofol dimer complex. Further results suggest strong CH−π interaction with weak hydrogen bonds between the molecules and water.[61] Interestingly, the water network near propofol plays an important role in the binding of general anesthetics to proteins. Using NMR spectroscopy, Wang et al. have reported that the critical amount of hydration water is absolutely essential for anesthetic−protein binding.[62]

Molecular dynamics (MD) simulation studies can assist in solving many unsolved issues regarding the in-depth insight into molecular interactions and the nature of the dynamics of water near propofol at the microscopic level. In recent past, Klein and co-workers have conducted MD simulation studies to investigate the mechanistic aspects of general anesthetics isoflurane and propofol action on prokaryotic pentameric channel GLIC.[63] They reported that both the molecules show pore inhibition mechanism at the micromolar concentrations and have a higher affinity in the unoccupied pore as compared with the allosteric site. In 2018, Wang et al. have reported various propofol binding sites in NaChBac using molecular docking and MD simulation studies.[24] However, Henin et al. have used an alchemical free energy perturbation technique to calculate affinities for isoflurane binding to apoferritin, which compared well to experiment.[64] Further, Tang and co-workers have reported the nature and locations of halothane interactions using flexible ligand docking to their model of the $\alpha_4\beta_2$ nAChR in an open conformation.[65] The binding free energy calculation shows that halothane binds with a low affinity to most sites. So, the atomistic level investigations including propofol and several other anesthetic molecules have begun to be more prominent in recent years by employing the MD simulation technique.[66] In early research work, Koubi et al. have shown that the presence of anesthetic molecules alters the membrane structural properties.[67] They observed that the presence of the molecule led to a large perturbation of the electrostatic potential across to the membrane interface, as well as the substantial increase in the microscopic viscosity of the lipid core compared with the pure lipid bilayer. The observed perturbations of the lipid membranes in the presence of anesthetics are showing the difference in their physiological effects as compared to the nonimmobilizers. Interaction of anesthetic molecules propofol and fentanyl with lipid bilayer (DOPC and DPPC) have been studied using atomistic simulation.[68] The increased content of propofol in the DPPC bilayer causes the decrease in isothermal compressibility modulus along with decrease of melting temperature.[69] Umbrella sampling simulation studies suggests the partition of propofol into a gel DPPC phase is not favorable, and it is mainly enthalpy driven at the polar region.[70] Ahmad et al. have conducted the coarse-grained simulation to study the propofol within the quaternary ammonium palmitoyl glycol chitosan micelle solution and found a heterogeneous distribution within the micellar population.[71] Importantly, the solubility of anesthetics in deep eutectic solvent has also been explored using theoretical calculations.[72]

Despite being widely used and studied, understanding the solvation processes of propofol in aqueous medium remains

https://doi.org/10.1021/acs.jpcb.3c04932
J. Phys. Chem. B XXXX, XXX, XXX−XXX

Table 1. Details of MD Simulations of Propofol/PG/Water Mixtures

	PFL/PG/water						
system	PG	water	PFL	f (V/V)	PG slab (nm)	water slab (nm)	box dimension (nm)
S1	1033	2994	7	1.4	6 × 6 × 3.5	6 × 6 × 2.5	6 × 6 × 6
S2	886	3592	7	1.0	6 × 6 × 3	6 × 6 × 3	6 × 6 × 6
S3	738	4192	7	0.7	6 × 6 × 2.5	6 × 6 × 3.5	6 × 6 × 6
S4	590	4790	7	0.5	6 × 6 × 2	6 × 6 × 4	6 × 6 × 6
S5	148	6587	7	0.1	6 × 6 × 0.5	6 × 6 × 5.5	6 × 6 × 6

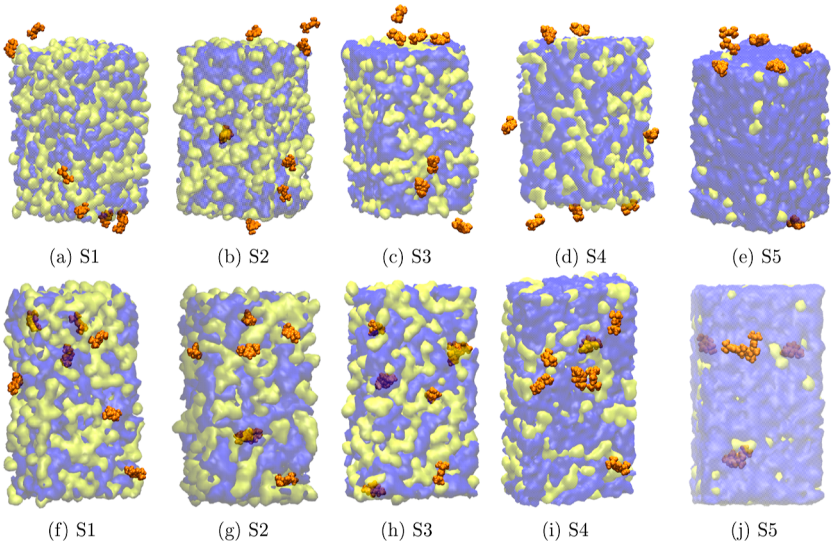

Figure 1. Snapshots of the configuration correspond to five different (Table 1) simulated systems at the beginning (equilibrated PG/water mixture and propofol) and at the end of the simulation. Yellow and blue color surface plot represents PG and water molecules, whereas the propofol molecules are represented by vdW plots with brown color.

elusive and has not achieved the same degree of knowledge as aspects derived from pharmaceutical evolution. It is well accepted that the molecular aggregation/dissolution process is partially controlled by the nature of the water microstructure around the propofol. So, the characterization of the microsolvation shell of propofol can explore the hidden truth that plays a vital role in determining the stability of the drug (propofol) solubilized in the binary mixture is important. To the best of our knowledge, these facts have not been investigated in detail and require more attention.

To investigate the differential behavior of water microsolvation shells around propofol, we have performed atomistic MD simulations of five different compositions of PG/water mixture containing propofol molecules. In this work, we have calculated various correlation functions including the ones that give information regarding the structural arrangement of molecules within the system including the radial distribution function. Rotational correlation and mean squared displacement have been calculated to investigate the dynamics of water in the propofol microsolvation shells for all five compositions, followed up with the dynamics of hydrogen bond formed between propofol and water molecules and the intermittent residence time correlation function. This article is organized as follows: starting with the discussion of simulation and its methods that have been employed in the current study, including the force fields. The detailed investigation of structural and dynamical properties, as observed during the simulation, has been reported in the form of snapshots followed by reporting the various correlation function analysis and their interpretation. In the last section, we summarize the important findings from our study.

METHODOLOGY

System Setup and Simulation Details. Initially, we have constructed cubic simulation box containing a PG−water binary mixture with propofol molecules for individual compositions using the GROMACS tools,[73,74] the approximate dimension and compositions are listed in Table 1, where we have opted for seven propofol molecules for the individual simulation system, and the S2 simulation setup is based on the experimental report by Trapani and co-workers,[35] along with other compositions (Table 1). For Bulk water, a cubic box of 1054 water molecules was built separately. The CHARMM general force field was used to obtained the PG parameters.[75,76] The CHARMM modified TIP3P water model was used to model the solvent,[77] and the CHARMM-consistent propofol parameters were taken from a recent study.[63] The simulation experiments on the constructed systems were initiated by removing the unfavorable contacts via steepest descent energy minimization. This was followed by a rapid equilibration at a constant temperature (T = 300 K) and volume (NVT). Each NVT equilibration was carried out for 10 ns duration, followed up with a constant temperature (T = 300 K) and pressure (P = 1.0 atm) and NPT simulation run for 20 ns. The final equilibration of the system was continued via a production run of 100 ns in the NPT ensemble, with simulated trajectories stored at every 100 ps. Structural properties can be calculated from a 100 ns NPT simulation. For investigating the coordination number, diffusion, hydrogen bond relaxation,

https://doi.org/10.1021/acs.jpcb.3c04932
J. Phys. Chem. B XXXX, XXX, XXX−XXX

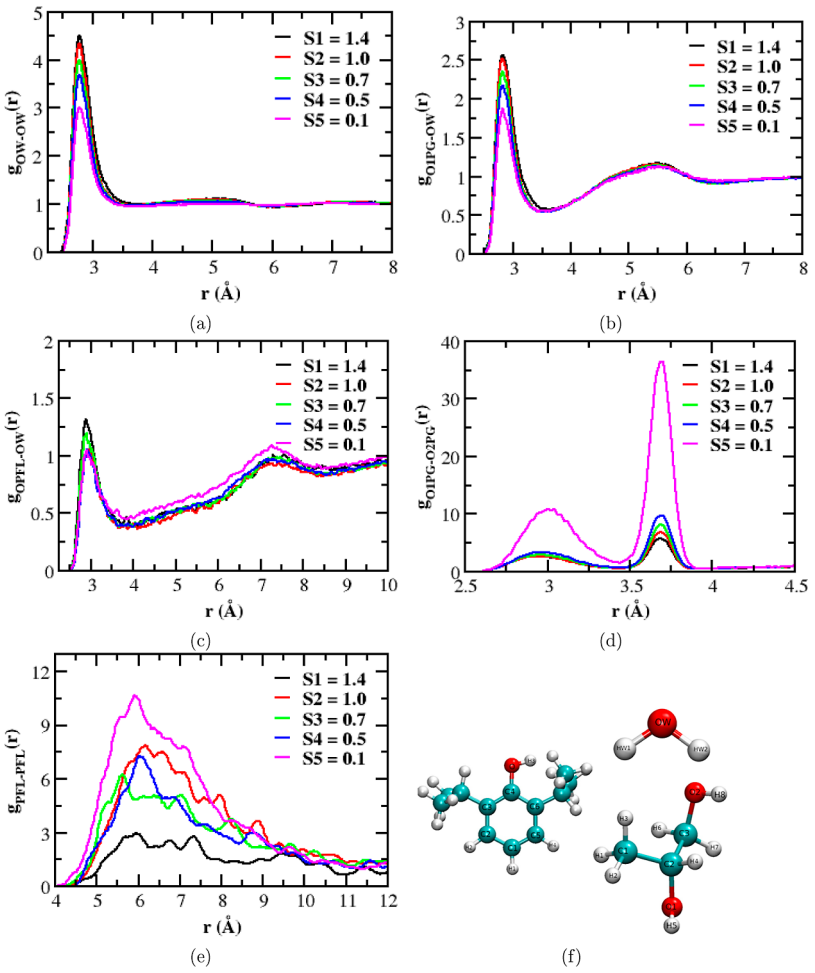

Figure 2. Radial distribution functions between the (a) oxygen atoms of water molecules, $g_{OW-OW}(r)$, (b) oxygen atom (O1) of the PG and water oxygen (OW) atom, $g_{O1PG-OW}(r)$, (c) oxygen atom (O) of the propofol and water oxygen (OW) atom, $g_{OPFL-OW}(r)$, (d) oxygen (O1)−oxygen (O2) of PG hydroxyl oxygen atoms, $g_{O1PG-O2PG}(r)$, (e) center of mass of propofol molecules, $g_{PFL-PFL}(r)$ for five different compositions (Table 1) of PG/water mixture. (f) Ball and stick representation of various constituents present in the proposed compositions (Table 1), with atom labeling.

residence time correlation, and reorientational aspects of water molecules, a 1 ps resolution *NVT* run was further carried out for 10 ns duration. Additionally, 5 fs high-resolution trajectory of 50 ps time was also generated to probe the ultrafast translational and dynamical aspects of water.

We carried out all atom MD simulations corresponding to the varied composition of PG/water binary mixtures with propofol (Table 1) using the 2018.3 version of the parallel MD simulation package GROMACS.[73,74] In the whole course of simulations, the LINCS algorithm[78] was employed for bond constraints. Leap-frog integrator was used to solve Newton's equation of motion to generate the time reversible trajectory. The Verlet cutoff scheme was used for neighbor list generation with a cutoff of 1.2 nm with every 10 step neighbor list update. A cutoff radius of 1.2 nm was used for all van der Waals interactions, and standard long-range corrections have also been taken into consideration. The long range electrostatic interactions were treated using the Particle Mesh Ewald method,[79,80] with cubic interpolation of the order of 4 and a Fourier spacing of 0.16 nm. In our simulations, we employed 1.2 nm for the real space cutoff. Temperature coupling in the *NVT* and *NPT* runs were provided via a velocity rescaling thermostat[81,82] of relaxation time, 1.0 ps, where the velocities are scaled by *a* factor λ in order to attain desired temperature quickly. The velocity rescale thermostat is a modified Berendsen thermostat with a stochastic term added that ascertain correct kinetic energy distribution has been achieved and proper canonical ensemble is generated.[81,82] Whereas pressure coupling in the system was provided by Parrinello−Rahman Barostat[83,84] with a isotropic coupling constant of 1.0 ps and a compressibility factor of 4.5×10^{-5} bar^{-1}. All of the simulation boxes followed the three-dimensional periodic boundary conditions, with the 2 fs time step of simulation. All of the images are produced using VMD.[85]

RESULTS AND DISCUSSION

Structural Inspection: a Molecular Level Heterogeneity. The configurations of five different simulated systems at the beginning and at the end of the simulation are displayed in Figure 1. It is clear from the figure that the propofol in the PG/water binary mixture shows the modulation of structure formation and clustering with varying composition (Table 1) during the nanosecond time scale of the simulation. The important notable feature from Figure 1 is that, as the simulation progresses, the segregation happens at the microscopic level differently as per their composition. This is in contrast to an almost zero segregation and distinct liquid composition at the beginning.

https://doi.org/10.1021/acs.jpcb.3c04932
J. Phys. Chem. B XXXX, XXX, XXX−XXX

Several groups have recently tried to unfold the microscopic interaction behavior of water and PG in solution[86,87] and reported water−PG interaction is more preferred in 30 mol % solution over PG−PG self-interaction and the similar observation has been reported for 50 mol % solution.[87] Observations of water clustering behavior in the presence of small amphiphilic molecules such as methanol, dimethyl sulfoxide (DMSO), and glycerol has long been known.[17,18,88]

It is evident from the beginning and end of the simulation snapshots for various compositions that the PG at low molecular ratio form clusters and tends to interact more with itself than with water, and in such a case, the propofol molecules shows a tendency to form aggregates, which may reduce their solubility in the PG/water binary mixture (S5). Interestingly, at higher PG composition ratio (S1), the water in the binary mixture favors the extended chainlike[89] connectivity and the propofol prefers the dispersed state. In the system S2, the similar dispersion behavior of propofol has been observed as like S1, and the water molecules tend to form both cluster and chainlike networks[89] that percolate within the PG matrix. So, the higher propylene glycol vol/vol % ratio indicates the augmented tendency of the formation of chainlike water networks in the PG/water binary mixture. To gain further insight into this initial observation, we have carried out the structural characterization of the PFL−PG−water mixture, along with the microscopic dynamics of water near propofol for the mentioned compositions (Table 1).

Radial Distribution Function. The structure and dynamics of water around the drug-like molecules (propofol) play an important role in determining their solubility in the binary solution (PG/water mixture). We have observed in the previous section that the propofol molecules in the lower PG content (S5) show aggregation behavior, which is less probable in the higher PG content (S1). Such a molecular level observation dictates the solubility of the drug-like molecules in the binary mixtures. So, it would therefore be interesting to examine the structure of water around propofol (PFL) and PG, and the structure of itself (PFL−PFL, PG−PG) with the variation of compositions. With this aim, we have estimated the radial distribution functions (eq 1) for OW (water)−OW (water), O1 (PG)−OW (water), O (PFL)−OW (water), O1 (PG)−O2 (PG), and center of mass (PFL)−center of mass (PFL) atom pairs and plotted in Figure 2a−e, respectively.

$$g_{mn}(r) = \frac{V}{N^2}\left\langle \sum_{i}^{N_m}\sum_{j}^{N_n}\delta(r - r_{ij})\right\rangle \quad (1)$$

The radial distribution function, $g_{mn}(r)$, determine the distribution of an atom of type n from a reference atom of type m.[90]

In Figure 2a, we present the radial distribution functions between oxygen atoms of water molecules, $g_{OW-OW}(r)$, for five different compositions (Table 1). The first peak is nearest around 0.28 nm, indicates the well-defined first solvation shell around water oxygen (OW), followed by the unstructured second solvation shell, reported for the TIP3P water model.[77] The intensity of the first peak and the first part up to 0.35 nm of the pair correlation functions truly depend on the PG content of the PG/water mixture. In $g_{OW-OW}(r)$, the first peak intensity is an implication of a more structured water network for higher PG content. Similar observation for solvent peak maxima enhancement with increase in solute concentration was reported in several other works.[91−93]

In Figure 2b, we display the radial distribution function between the oxygen atom (O1) of the PG and water oxygen (OW) atom, $g_{O1PG-OW}(r)$, for five different compositions (Table 1). The major characteristic of $g_{O1PG-OW}(r)$ for five different compositions is a well-defined first peak with altered intensity centered on 0.28 nm which indicates that the water corresponding to the first peak is more structured near O1PG for high PG content, and the change in intensity is most probably due to the competitive nature of hydrophilic PG cluster formation by varying their composition in the PG/water mixture. In a report, Egorov et al. have observed the similar trends for other binary mixtures.[94]

The first peak of $g_{OPFL-OW}(r)$ between the oxygen atom (O) of the propofol and water oxygen (OW) atom for five different compositions is shown in Figure 2c, with the position of the peak centered at 0.29 nm. The altered intensity of the first peak implies that the water in the first solvation of OPFL is more structured for higher PG vol/vol % ratio. The hydrophilic PG influences the stability of the water network as well as the stability of the microsolvation shell around propofol, which may play a key role in the propofol dissolution process.

The distinctive features for oxygen (O1)−oxygen (O2) pair correlation function $[g_{O1PG-O2PG}(r)]$ of PG hydroxyl oxygen atoms are observed in Figure 2d for five compositions, with the position of the peak centered at 0.3 nm followed by an interesting feature between 0.34 and 0.39 nm. In the pair correlation functions, the first peak corresponds to intra- and intermolecular O1−O2 interactions, whereas the stepwise reduction of second peak intensity corresponds to intermolecular O1−O2 interactions for five different PG/water compositions. At low PG content (S5), the interaction between different PG hydroxyl oxygens is enhanced as observed in the peak intensity. The enhancement of peak intensity at low PG content (S5) suggests the significant self-clustering of PG. In Figure 2b, we showed the $g_{O1PG-OW}(r)$ between PG oxygen (O1PG) and water oxygen (OW) atom, which indicates that the PG prefers to be associated with water rather than to itself at higher PG content in the PG/water mixture.

In Figure 2e, we displayed the pair correlation function $[g_{PFL-PFL}(r)]$ between the center of mass of propofol molecules for the mentioned compositions (Table 1). The $g_{PFL-PFL}(r)$, shows a broad complicated structure between 0.4 and 1.0 nm, and the contrasting intensities of the peak implies that the propofol molecules are forming aggregates for low PG content (S5), whereas the aggregation tendency becomes weaker for higher PG content in PG/water mixture (S1). In Figure 2b, the pair correlation function, $g_{O1PG-OW}(r)$, implies that the water is more structured for high PG content, and the similar trends of the water network observed in $g_{OPFL-OW}(r)$ (Figure 2c) which implies that the highly structured microsolvation shell around propofol may retard the aggregation process for larger PG content (S1). Conversely, the less ordering of the microsolvation shell around propofol may facilitate the aggregation process for reduced PG content. Therefore, the microsolvation shell around the propofol should be more structured for a successful dissolution process.

Water Microsolvation. The potentially different water around the propofol for various compositions plays a vital role in controlling their solubility in the PG/water mixture. The differential nature of the water microstructure can influence both translational and reorientational dynamics of water next to the propofol, which is likely to control their solubility. In

https://doi.org/10.1021/acs.jpcb.3c04932
J. Phys. Chem. B XXXX, XXX, XXX−XXX

this section, we examine the dynamics of water near propofol for five different compositions.

Mean Square Displacements. The translational mobility of water molecules can be studied by monitoring the diffusion coefficient (D) which can be obtained from the slope of the mean square displacement (MSD) vs time curve, using the well-known Einstein relation.[95]

$$D = \lim_{\delta t \to \infty} \frac{\langle |r(t) - r(0)|^2 \rangle}{2n\delta t} = \lim_{\delta t \to \infty} \frac{\langle \Delta r^2 \rangle}{2n\delta t} \quad (2)$$

where n is the dimensionality of the system, and $r_i(0)$ and $r_i(t)$ are the coordinates of the ith water molecule oxygen atom at times $t = 0$ and $t = t$, respectively. The averaging $\langle .. \rangle$ is done over both time origins and water molecules.

We have calculated the MSDs of water molecules present in the microsolvation shell around the propofol for five different compositions (Table 1), which are displayed in Figure 3. In the

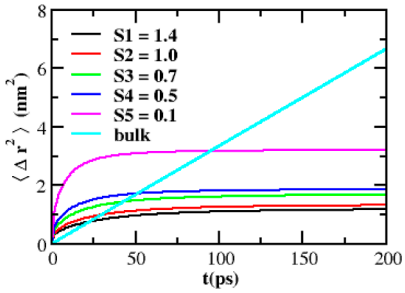

Figure 3. MSD of the water molecules present in the microsolvation shell of propofol. Water molecules that reside within 5 Å from the hydroxyl oxygen atom of propofol are considered for calculation. For comparison, the MSD of the bulk water molecules is also incorporated.

calculations, we have considered only those water molecules, which reside within 5 Å from the hydroxyl oxygen atom of the propofol, defined as the microsolvation shell. For comparison, we have incorporated the MSD for bulk water molecules, shows the water diffuse with a self-diffusion coefficient of 5.22 × 10^{-5} cm^2/s at 300 K. It is clear from the figure that the translational diffusion of water belongs to the microsolvation shell of the propofol which shows flat MSD curves for all five compositions and indicates the highly ordered water microstructure network as compared to the bulk (Figure 2a). Such ordered phases exhibit damped diffusion, with minor displacement due to thermal agitation and orientational disordering caused by the presence of two isopropyl groups ortho to the hydroxyl group of propofol. Importantly, the MSD of water belonging to the microsolvation shell of propofol for five different compositions is significantly different from one another, and the MSD curve of water for low PG content (S5) is higher as compared to the other compositions, exhibiting the higher molecular libration against the equilibrium position of water that arrested with increasing the PG content in PG/water mixture. However, the plateau in MSD reflects the availability of the space in the microsolvation structure around propofol for low PG content is larger, and increasing the PG content the water microstructure favors dense packing with lesser availability of space and restricted translation. Recently, Henao et al. have reported the similar diffusive behavior of water for various crystal phases.[96] Again, the water diffusion shows a variable dependence of the PG content in the PG/Water mixture, and the sluggish diffusion of water for high PG content due to the dominant role of PG−water interactions favor the dense packing of water microstructure around the propofol. In the recent past, Cerveny et al. have observed the dielectric response of *n*-PG−water mixture, where restricted water mobility has been observed below critical water concentration.[50] They have shown that as the concentration of water molecules starts increasing more and more, the interactions within the water molecules increase as compared to *n*-PG−water interactions. Interestingly, there is a marked decrease in the mobility of water as the PG fraction in the solution increases. Similar observation of water diffusion with varied composition was reported by Luzar and Chandler[97] in their simulation study on the DMSO−water mixture.

The water mobility in the propofol microsolvation shell for low PG content (S5) is higher as compared to the other compositions (Table 1), whereas for higher PG content, (S1) the water mobility is reduced. Such differential water mobility agrees well with the water microstructure around propofol which indicates the higher ordering of water microsolvation shell around propofol, as observed in the previous section for S1, depicts the restricted mobility of water in the propofol microsolvation shell (Figure 3), and results in the hindered aggregation or favored dissolution process of propofol. However, the lower ordering of microsolvation shell around propofol, as observed in the previous section for S5, illustrates the unrestricted dynamics of water in the propofol microsolvation shell (Figure 3) and facilitates the aggregation process of propofol.

Reorientational Dynamics. In a varied composition of binary mixture containing drug-like molecules (propofol), the reorientational dynamics of water in the microsolvation shell of the molecule can be influenced remarkably. A water molecule can switch its orientation by changing the hydrogen bond formed with the acceptor or donor molecule, and its orientation often gets restricted in the presence of confinement, which can be geometric or electrostatic in nature, except for subpicosecond libration motion which is possible due to the tumbling motion of broken hydrogen bond or any of free OH hand of water molecule. Therefore, rotation of water requires an exchange event and that can be hindered in the case where such exchange is less probable leading to retardation. The rotational motion of water can be monitored by calculating the reorientational dynamics of the OH vector of water. The time evolution of the OH vector of water can be monitored by calculating the orientational time correlation function which can be decayed to zero for orientationally disordered phases, but on the other hand, for orientationally ordered phases, the orientations are correlated with one. The orientational time correlation function $C_l(t)$, is defined using the following equation

$$C_l^{\mu}(t) = \langle P_l[\mu(0)\cdot\mu(t)] \rangle = \langle P_l[(\cos\theta(t))] \rangle \quad (3)$$

where l is the order of legendre polynomial

$$P_1(x) = x \quad (4)$$

$$P_2(x) = (3x^2 - 1)/2 \quad (5)$$

and μ represents the vector of orientation in the molecule used for the calculation. The angular brackets indicate that the averaging is over both the water molecules and time origins. Again, the calculated reorientation time can be correlated with experiments such as $C_1(t)$ is observed in dielectric spectros-

https://doi.org/10.1021/acs.jpcb.3c04932
J. Phys. Chem. B XXXX, XXX, XXX−XXX

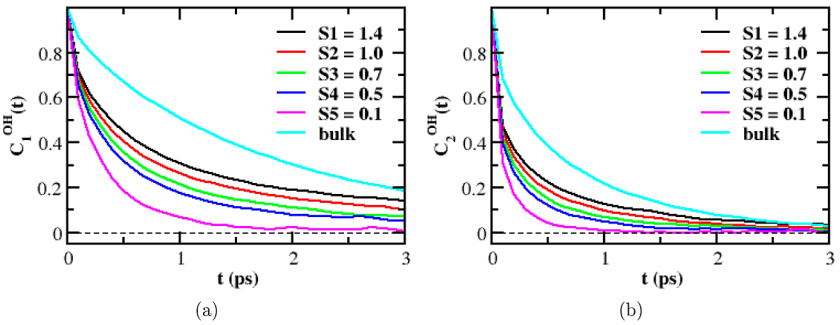

Figure 4. Reorientational time correlation functions of the water OH vector, (a) $C_1^{OH}(t)$ and (b) $C_2^{OH}(t)$, for the water present in the microsolvation shell around the propofol for five different compositions. The relaxation for bulk water molecules is incorporated for comparison.

copy, and $C_2(t)$ is observed in NMR and light scattering experiment.[95]

To investigate the effect on rotational behavior of water present in the microsolvation shell around the propofol for all five compositions, the first and second order Legendre orientational correlation function (OCF) of the OH vector of water has been calculated and presented in Figure 4. For comparison, we have also introduced the correlation function for bulk water molecules. It is evident from the figure that the water reorientation becomes slower as the PG/water mixture composition tends toward high PG content. However, the OCF relaxation of the microsolvation shell water for all five compositions is faster as compared to the bulk water which can be interpreted from the fact that the bulk water has orientational and translational motions coupled. Such molecular coupling becomes weaker for water belonging to microsolvation shells. Because they usually utilize their energy for molecular rotation and very minimal for translation. The rotational behavior of water follows a monotonic composition dependence, suggests the faster OCF decay of water correspondence to the unstable water microsolvation shell near the propofol for low PG content (S5), as discussed in the earlier section. Such unstable water microsolvation shells near the propofol favored their aggregation behavior. The damped reorientation of water in the propofol microsolvation shell for large PG content (S1) signifies the stable water micronetwork around the propofol, which truly depends on the PG−water interactions, discussed earlier. In the higher concentration of PG, small pockets of water network are formed where propofol resides and is solvated in those pockets, and the dissolution process is expedited.

The OCFs shown in Figure 4, can be expressed as an exponential function $e^{-t/\tau}$, and the ratio between the first and second order reorientation times (τ_1/τ_2) provides information about the kind of the orientation. The more diffusive molecular rotation consist of small amplitude angular jumps,[98] and the OCF decay can be expressed exponentially with the following equation

$$C_l^{\mathrm{OH}}(t) = e^{-l(l+1)D_{\mathrm{rot}}t} \tag{6}$$

and the relaxation time as

$$\tau_l^{-1} = l(l+1)D_{\mathrm{rot}} \tag{7}$$

with ratio $\tau_1/\tau_2 = 3$ and verifying this value signify the rigorous test for the Debye model. The rotations consistent with small angular jumps corresponds to higher τ_1/τ_2 values, and the large angular jumps corresponds to the smaller τ_1/τ_2 values.

In Figure 5, we displayed the ratio of τ_1/τ_2, for bulk water, the value is closer to 2 in the long time limit, and for propofol

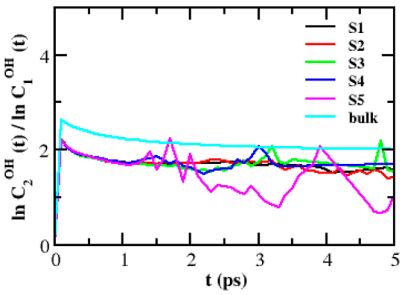

Figure 5. Ratio of first and second order reorientation times $[\ln(C_2^{OH}(t))/\ln(C_1^{OH}(t)]$ of the OH vector for the water molecules belongs to the microsolvation shell around the propofol for five different compositions. The ratio for bulk water molecules is incorporated for comparison.

microsolvation shell water, the value deviating slightly from which indicates that the reorientation in the water microsolvation shells take place for large-amplitude angular jumps, as observed in the bulk water.[99] The smaller values of the ratio for water are monitored previously.[100−102] Importantly, the deviation of ratio τ_1/τ_2 from the bulk value $(\tau_1/\tau_2 \approx 2)$ for propofol microsolvation shells may alter the hydrogen bond lifetime, and in the next subsection, the hydrogen bond dynamics between propofol and water molecules belongs to the microsolvation shells and its conceptual implications for propofol dissolution process will be discussed.

Hydrogen Bond Dynamics. The water microstructural network and the dynamics of water molecules present in the propofol microsolvation shell are influenced by the isopropyl groups ortho to sterically hindered hydroxyl group, and the steric hindrance by two alkyl groups hindered the formation of hydrogen bond in aqueous medium. So, the hydrogen bond dynamics play a vital role in determining the solubility of propofol molecules in PG/water mixtures. The hydrogen bond can be defined as either a geometric[103−105] or an energetic[106] criteria. However, we have opted for geometric criteria to define a hydrogen bond.[103−105]

To observe the structural relaxation of hydrogen bonds, one can use the time correlation function, defined as[107]

$$C_{\mathrm{HB}}(t) = \langle h(t+\tau)h(\tau)\rangle / \langle h(\tau)h(\tau)\rangle \tag{8}$$

where the dynamical variable $h(t)$ is equal to unity for a specific pair of propofol−water or water−water sites is hydrogen bonded at time t and is zero otherwise. In this

https://doi.org/10.1021/acs.jpcb.3c04932
J. Phys. Chem. B XXXX, XXX, XXX−XXX

work, we have opted purely geometric criteria to define a hydrogen bond, the propofol−water pair is considered to be hydrogen bonded, if the O (PFL)−OW and O (PFL)−HW1/HW2 distances are smaller than 0.35 and 0.25 nm, respectively, and the O (PFL)−OW−HW1/HW2 angle is smaller than 30°, and the water−water pair is treated to be hydrogen bonded, if the OW−OW distance is smaller than 0.35 nm and the OW−OW−HW1/HW2 angle is smaller than 30°.[104,105] The angular brackets indicate averaging over all pairs of hydrogen bonds and over τ (initial times). The $C_{HB}(t)$ designates the probability that the hydrogen bond between the specific propofol−water or water−water pair is intact at time $t + \tau$ ($h(t + \tau) = 1$), given it was intact at time τ ($h(\tau) = 1$). So, the $C_{HB}(t)$ allows reformation of the broken bond, which loses the hydrogen bond criteria at some intermediate time. Thus, it allows recrossing the bonded and nonbonded states energy barrier. It also measures the correlation of hydrogen bonds independent of possible bond breaking events, and commonly termed as "intermittent hydrogen bond correlation function".[107,108] Importantly, the $C_{HB}(t)$ relaxation gives information about the structural relaxation of a hydrogen bond pair.

In Figure 6, we showed the time correlation function for the hydrogen bond formed between the propofol and the water

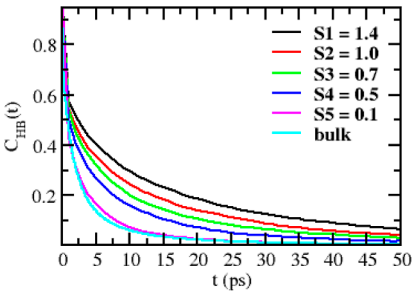

Figure 6. Intermittent hydrogen bond time correlation function, $C_{HB}(t)$, for the hydrogen bonds formed between the propofol and the water molecules present in the microsolvation shell around the propofol for all five compositions. The same for the water−water hydrogen bond for bulk water molecules is incorporated for comparison.

molecules present in the microsolvation shell around the propofol for five different compositions (Table 1). The same for the hydrogen bond formed between a pair of bulk water molecules is included for comparison. The $C_{HB}(t)$ for bulk water was estimated from a MD simulation of TIP3P water under similar thermodynamic conditions. It is noticed from the figure that the structural relaxation of the propofol−water hydrogen bond is slower as compared to the bulk water counterpart. Interestingly, the figure exhibiting the propofol−water hydrogen bond relaxation for all five compositions is notably different from one another, and the relaxation for higher PG content (S1) is slower as compared to the rest. The relaxation pattern clearly indicates the existence of slow components for all five compositions, which can be described by multiexponential law.[103] Figure 6 resembles the contrasting rigidity of the microsolvation shells around propofol for five different compositions. Further, the structural relaxation of the hydrogen bonds formed between propofol and water belongs to microsolvation shells, which shows a variable dependence of the PG content in the PG/water mixture and the slower relaxation of propofol−water hydrogen bonds for high PG content (S1) because of the major role played by PG−water interactions, which influences the formation of an ordered water microstructure network around propofol for S1 and S2 and restricts the mobility of water in the microsolvation shells. Again, the relaxation behavior toward low PG content is faster with respect to the other compositions (Table 1). Such a key observation agrees nicely with the decreasing trends of ordering of the water microsolvation shell around propofol for lowering the PG content in the PG/water mixture, which is in accordance with faster reorientation of the microsolvation shell water for S4 and S5, observed in a previous section, favoring the aggregation process of propofol at low PG content.

Residence Time. The residence time provides information about the dynamical nature of the water microstructure around propofol. The differential behavior of the water microstructure around propofol is due to varying interactions of water with PG in different compositions of the PG/water mixture. Thus, the altering PG−water interactions can give rise to unusual structural relaxation of the water microsolvation shell around propofol for five different compositions. To characterize the structural relaxation of the microsolvation shell around the propofol molecule, we have constructed the intermittent residence time correlation function, $R(t)$, which describes the probability that a particular molecule stays in a given region at time t, given it existed at the initial time. We defined the intermittent residence time correlation function as

$$R_j(t) = \frac{\langle \theta_j(\tau)\theta_j(t+\tau) \rangle}{\langle \theta_j(\tau)\theta_j(\tau) \rangle} \tag{9}$$

where the population variable $\theta_j(t)$ is unity when the molecule r_i is present in a given region j at time t, and zero otherwise. So, during simulation, individual molecules can exit and enter in different regions, and the above correlation function is developed based on the residence time of all molecules present in the region j. The angular brackets denote averaging over all molecules present in the particular region and over initial times τ. The correlation function $R_j(t)$ describes the probability that a particular molecule stays in a given region j at time $t + \tau$ ($\theta_j(t + \tau) = 1$), given it exited at time τ ($\theta_j(\tau) = 1$). So, the $R_j(t)$ allows the revisit of the molecule that exits at the intermediate time from region j. Thus, the intermittent residence time correlation function, $R_j(t)$, estimates that the correlation of molecular residence at region j is independent of possible entry-exit events in the particular region. Therefore, the relaxation of $R_j(t)$ furnishes information about the structural mobility of a specific region.

We have measured the intermittent residence time correlation function, $R_{MS}(t)$, for the water molecules belonging to the microsolvation shell around the propofol for all five compositions, as displayed in Figure 7. In the calculations, we have opted only for those water molecules present within 5 Å from the hydroxyl oxygen atom of propofol, defined as the region for residence time estimation (j). For comparison, we incorporated the same for bulk water molecules. It is clear from the figure that the relaxation for all five compositions shows a faster short time decay followed by a long time tail. The initial rapid relaxation is due to the molecular libration, which moves the boundary molecules out of the defined region because of short displacements. However, the origin of the long time decay comes from the structural relaxation of the microsolvation shell around the propofol. So, the observed relaxation

https://doi.org/10.1021/acs.jpcb.3c04932
J. Phys. Chem. B XXXX, XXX, XXX−XXX

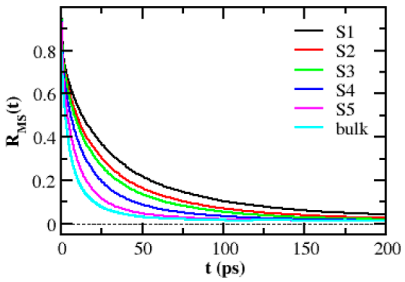

Figure 7. Intermittent residence time correlation function, $R_{MS}(t)$, for the water molecules present in the microsolvation shell around the propofol for five different compositions (Table 1). The same for bulk water molecules is incorporated for comparison.

of $R_{MS}(t)$ cannot be modeled by a single-exponential law. The sum of three exponentials (eq 10) has been used to model the distribution of residence times as well as the long time decay. The parameters for the best fit are displayed in Table 2.

$$R_{MS}(t) = a1^* e^{-(t/\tau_1)} + a2^* e^{-(t/\tau_2)} + a3^* e^{-(t/\tau_3)} \quad (10)$$

$$\langle \tau_{residence} \rangle = \frac{\sum_{i=1}^{3} a_i \tau_i}{\sum_{i=1}^{3} a_i} \quad (11)$$

It appears in the multiexponential fit that the $\langle \tau_{residence} \rangle$ value of the water microsolvation shell around propofol for all five compositions is higher than the bulk water. Again, the relaxation of $R_{MS}(t)$ for the water microsolvation shell around the propofol for all five compositions is remarkably different from one another, and the existence of short and long time components. As mentioned above, the presence of the long time decay due to the structural relaxation of the water microstructure present around the propofol. Further, we need to explore this aspect more microscopically. The multiexponential fit, Table 2, displayed the average intermittent residence time relaxation ($\langle \tau_{residence} \rangle$) for water belongs to the microsolvation shell around propofol for S1 is approximately three times higher in comparison to S5. Such remarkably slower relaxation due to the substantial contribution of the long time component of about ($a3^*\tau_3$ = 26.82 ps) for microsolvation water around S1, which is larger than that of the other four compositions [18.35 ps(S2), 15.24 ps(S3), 10.34 ps(S4), 6.89 ps(S5)]. So, the high PG content (S1) shows the slower structural relaxation of the microsolvation shell around propofol, which turns into faster relaxation as the PG content approaches low concentration. However, the $R_{MS}(t)$ relaxation depicts a dependence on PG content in the PG/water mixture, supporting the dominant role of the PG−water interactions in controlling the structural relaxation of the microsolvation shell which designates the slower structural relaxation of microsolvation shells around propofol, corresponds to the higher ordering of water microstructure and restricted water mobility, and results in the favorable dissolution process of propofol at higher PG content in PG/water mixture. On the other hand, the faster structural relaxation of the water microsolvation shell around propofol supports the lower ordering of water microstructure and unrestricted water dynamics in the microsolvation shell, preferring the aggregation process at low PG content in the PG/water mixture.

CONCLUSIONS

In this paper, we have studied in detail the structure and dynamics of water present in the microsolvation shells around propofol for five different compositions (Table 1). The simulation studies revealed that the propofol in the PG: water mixture modulates their internal structure formation, resulting in clustering with varying composition of PG content during the nanosecond time scale of the simulation. We monitored that the PG tends to interact more with itself than with water at the low molecular weight (PG) ratio in the PG/water mixture. However, the pair correlation function depicts a more ordered water microstructure around propofol for high PG content in the PG/water mixture. Hence, the hydrophilic PG controls the stability of the water network in the mixture, resulting in the ordered structure of the water microsolvation shell around propofol that plays a crucial role in the PFL dissolution process. We noticed that the translational and rotational behavior of water belonging to the propofol microsolvation shell is restricted for high PG content (S1), whereas the water mobility is relaxed toward the low PG content in the PG/water mixture. The structural relaxation of the hydrogen bond formed between the propofol and the water molecules present in the microsolvation shell around the propofol for five different compositions is found slower as compared to the bulk water and distinct from one another. We also observed that the structural relaxation of the mentioned hydrogen bond for higher PG content (S1) is slower compared to the others, which tends to be faster in the direction of low PG content. So, the propofol−water hydrogen bond relaxation resembles the contrasting rigidity of the microsolvation shells around propofol for all five compositions. However, the intermittent residence time correlation function for the water molecules belonging to the microsolvation shell around the propofol for five different compositions displayed a faster short time decay followed up with a long time tail. The initial rapid relaxation corresponds to the molecular libration and the origin of the long time decay from the structural relaxation of the microsolvation shell around the propofol. Interestingly, the relaxation of water microsolvation shells around the propofol for all five compositions is distinguishable from one another, and the high PG content shows the slower structural relaxation

Table 2. Multiexponential Fitting Parameters for the Intermittent Residence Time Correlation Function of Water Molecules Belongs to the Micro-Solvation Shell of Propofol

system	$a1$	τ_1 (ps)	$a2$	τ_2 (ps)	$a3$	τ_3 (ps)	$\langle \tau_{residence} \rangle$ (ps)
S1	0.26	0.87	0.53	25.88	0.21	127.72	40.76
S2	0.28	0.98	0.56	22.10	0.16	114.68	31.00
S3	0.28	0.96	0.57	19.31	0.15	101.57	26.51
S4	0.30	0.89	0.60	15.56	0.10	103.37	19.94
S5	0.34	0.99	0.61	11.69	0.05	137.74	14.36
bulk water	0.20	0.25	0.50	3.77	0.30	18.38	7.45

https://doi.org/10.1021/acs.jpcb.3c04932
J. Phys. Chem. B XXXX, XXX, XXX−XXX

that turns faster as the PG content approaches a low value. The relaxation behavior depicts a dependence on PG content in the binary mixture, which supports the dominant role of the PG−water interactions in controlling the structural relaxation of the microsolvation shell. Although this aspect requires further verification and is under major examination in our laboratory. So, our observations designate that the slower structural relaxation of the microsolvation shell around propofol corresponds to the extensive ordering of water microstructure and restricted water mobility amd results in the favorable dissolution process of propofol at higher PG content in the PG/water mixture. However, the faster structural relaxation of the similar water environment supports the insignificant ordering of water microstructure and unrestricted water dynamics and facilitates the aggregation process of propofol at low PG content in the PG/water mixture.

AUTHOR INFORMATION

Corresponding Author

Sudip Chakraborty − *Department of Computational Sciences, School of Basic Sciences, Central University of Punjab, Bathinda 151401, India;* orcid.org/0009-0008-5104-4907; Email: sudip.chakraborty@cup.edu.in

Authors

Anupama Sharma − *Department of Computational Sciences, School of Basic Sciences, Central University of Punjab, Bathinda 151401, India*

Vishal Kumar − *Department of Computational Sciences, School of Basic Sciences, Central University of Punjab, Bathinda 151401, India*

Complete contact information is available at: https://pubs.acs.org/10.1021/acs.jpcb.3c04932

Notes

The authors declare no competing financial interest.

ACKNOWLEDGMENTS

This work was supported in part by generous grants from the University Grants Commission (UGC)-BSR Start-up grant [F.30-432/2018(BSR)], Central University of Punjab—Research Seed Money, Department of Science and Technology (DST) under Fast Track Scheme for Young Scientist (SB/FT/CS-158/2013), Government of India. A.S. thanks CSIR for providing a scholarship. S.C. is thankful to Prof. Raghavendra P. Tiwari, Vice Chancellor, Central University of Punjab Bathinda, for encouraging the research and providing the necessary facilities.

REFERENCES

(1) Fasinu, P.; Pillay, V.; Ndesendo, V. M.; du Toit, L. C.; Choonara, Y. E. Diverse approaches for the enhancement of oral drug bioavailability. *Biopharm Drug Dispos.* **2011**, *32*, 185−209.

(2) Das, T.; Mehta, C. H.; Nayak, U. Y. Multiple approaches for achieving drug solubility: an in silico perspective. *Drug discovery today* **2020**, *25*, 1206−1212.

(3) Chaban, V. V.; Savchenko, T. I.; Kovalenko, S. M.; Prezhdo, O. V. Heat-driven release of a drug molecule from carbon nanotubes: a molecular dynamics study. *J. Phys. Chem. B* **2010**, *114*, 13481−13486.

(4) Smith, D. J.; Shah, J. K.; Maginn, E. J. Molecular dynamics simulation study of the association of lidocainium docusate and its derivatives in aqueous solution. *Mol. Pharm.* **2015**, *12*, 1893−1901.

(5) Riveros-Perez, E.; Riveros, R. Water in the human body: An anesthesiologist's perspective on the connection between physicochemical properties of water and physiologic relevance. *Ann. Med. Surg.* **2018**, *26*, 1−8.

(6) Nury, H.; Van Renterghem, C.; Weng, Y.; Tran, A.; Baaden, M.; Dufresne, V.; Changeux, J.-P.; Sonner, J. M.; Delarue, M.; Corringer, P.-J. X-ray structures of general anaesthetics bound to a pentameric ligand-gated ion channel. *Nature* **2011**, *469*, 428−431.

(7) Willenbring, D.; Xu, Y.; Tang, P. The role of structured water in mediating general anesthetic action on $\alpha 4\beta 2$ nAChR. *Phys. Chem. Chem. Phys.* **2010**, *12*, 10263−10269.

(8) Li, C.; Xu, Q.; Chen, X.; Li, R. Bezafibrate in several aqueous mixtures of low alcohols: solubility, solvent effect and preferential solvation. *J. Chem. Thermodyn.* **2021**, *156*, 106208.

(9) Baksi, A.; Biswas, R. Does Confinement Modify Preferential Solvation and H-Bond Fluctuation Dynamics? A Molecular Level Investigation through Simulations of a Bulk and Confined Three-Component Mixture. *J. Phys. Chem. B* **2020**, *124*, 11718−11729.

(10) Sridhar, A.; Johnston, A. J.; Varathan, L.; McLain, S. E.; Biggin, P. C. The solvation structure of alprazolam. *Phys. Chem. Chem. Phys.* **2016**, *18*, 22416−22425.

(11) Aydi, A.; Ortiz, C. P.; Caviedes-Rubio, D. I.; Ayadi, C.; Hbaieb, S.; Delgado, D. R. Solution thermodynamics and preferential solvation of sulfamethazine in ethylene glycol+ water mixtures. *J. Taiwan Inst. Chem. Eng.* **2021**, *118*, 68−77.

(12) Holguin, A. R.; Delgado, D. R.; Martinez, F.; Marcus, Y. Solution thermodynamics and preferential solvation of meloxicam in propylene glycol+ water mixtures. *J. Solut. Chem.* **2011**, *40*, 1987−1999.

(13) Dasari, S.; Mallik, B. S. Solubility and solvation free energy of a cardiovascular drug, LASSBio-294, in ionic liquids: A computational study. *J. Mol. Liq.* **2020**, *301*, 112449.

(14) Huang, Y.; Ji, Y.; Zhang, M.; Ouyang, D. How imidazolium-based ionic liquids solubilize the poorly soluble ibuprofen? A theoretical study. *AIChE J.* **2020**, *66*, No. e16940.

(15) Kaiser, A.; Ritter, M.; Nazmutdinov, R.; Probst, M. Hydrogen bonding and dielectric spectra of ethylene glycol−water mixtures from molecular dynamics simulations. *J. Phys. Chem. B* **2016**, *120*, 10515−10523.

(16) Gubskaya, A.; Kusalik, P. Molecular dynamics simulation study of ethylene glycol, ethylenediamine, and 2-aminoethanol. 2. Structure in aqueous solutions. *J. Phys. Chem. A* **2004**, *108*, 7165−7178.

(17) Roy, S.; Bagchi, B. Solvation dynamics of tryptophan in water-dimethyl sulfoxide binary mixture: In search of molecular origin of composition dependent multiple anomalies. *J. Chem. Phys.* **2013**, *139*, 034308.

(18) Zhang, X.; Wang, Z.; Chen, Z.; Li, H.; Zhang, L.; Ye, J.; Zhang, Q.; Zhuang, W. Molecular Mechanism of Water Reorientation Dynamics in Dimethyl Sulfoxide Aqueous Mixtures. *J. Phys. Chem. B* **2020**, *124*, 1806−1816.

(19) Walsh, C. T. Propofol: milk of amnesia. *Cell* **2018**, *175*, 10−13.

(20) Adler, A. C. Propofol: review of potential risks during administration. *AANA J.* **2017**, *85*, 104.

(21) Garcia, P. S.; Kolesky, S. E.; Jenkins, A. General anesthetic actions on GABAA receptors. *Curr. Neuropharmacol.* **2010**, *8*, 2−9.

(22) Oakes, V.; Domene, C. Capturing the molecular mechanism of anesthetic action by simulation methods. *Chem. Rev.* **2019**, *119*, 5998−6014.

(23) Dutta, M.; Gilbert, S. P.; Onuchic, J. N.; Jana, B. Mechanistic basis of propofol-induced disruption of kinesin processivity. *Proc. Natl. Acad. Sci. U.S.A.* **2021**, *118*, No. e2023659118.

(24) Wang, Y.; Yang, E.; Wells, M. M.; Bondarenko, V.; Woll, K.; Carnevale, V.; Granata, D.; Klein, M. L.; Eckenhoff, R. G.; Dailey, W. P.; et al. Propofol inhibits the voltage-gated sodium channel NaChBac at multiple sites. *J. Gen. Physiol.* **2018**, *150*, 1317−1331.

(25) Lemaitre, F.; Hasni, N.; Leprince, P.; Corvol, E.; Belhabib, G.; Fillâtre, P.; Luyt, C.-E.; Leven, C.; Farinotti, R.; Fernandez, C.; et al. Propofol, midazolam, vancomycin and cyclosporine therapeutic drug monitoring in extracorporeal membrane oxygenation circuits primed with whole human blood. *Crit. Care* **2015**, *19*, 40−46.

(26) Thompson, K. A.; Goodale, D. B. The Recent Development of Propofol (DIPRIVAN®). *Intensive Care Med.* **2000**, *26*, S400−S404.
(27) McCulloch, M.; Lees, N. Assessment and modification of pain on induction with propofol (Diprivan). *Anaesthesia* **1985**, *40*, 1117−1120.
(28) Eriksson, M.; Englesson, S.; Niklasson, F.; Hartvig, P. Effect of lignocaine and pH on propofol-induced pain. *Br. J. Anaesth.* **1997**, *78*, 502−506.
(29) Wolf, A.; Weir, P.; Segar, P.; Stone, J.; Shield, J. Impaired fatty acid oxidation in propofol infusion syndrome. *Lancet* **2001**, *357*, 606−607.
(30) White, P. F. Propofol formulation and pain on injection. *Anesth. Analg.* **2002**, *94*, 1042.
(31) Rieschke, P.; LaFleur, B. J.; Janicki, P. K. Effects of EDTA-and sulfite-containing formulations of propofol on respiratory system resistance after tracheal intubation in smokers. *J. Am. Soc. Anesthesiol.* **2003**, *98*, 323−328.
(32) King, C. A.; Ogg, M. Safe injection practices for administration of propofol. *AORN J.* **2012**, *95*, 365−372.
(33) Baker, M. T.; Naguib, M.; Warltier, D. C. Propofol: the challenges of formulation. *J. Am. Soc. Anesthesiol.* **2005**, *103*, 860−876.
(34) Damitz, R.; Chauhan, A.; Gravenstein, N. Propofol emulsion-free drug concentration is similar between batches and stable over time. *Rom. J. Anaesth. Intensive Care* **2016**, *23*, 7.
(35) Trapani, A.; Laquintana, V.; Lopedota, A.; Franco, M.; Latrofa, A.; Talani, G.; Sanna, E.; Trapani, G.; Liso, G. Evaluation of new propofol aqueous solutions for intravenous anesthesia. *Int. J. Pharm.* **2004**, *278*, 91−98.
(36) Shityakov, S.; Salmas, R. E.; Durdagi, S.; Salvador, E.; Papai, K.; Yanez-Gascon, M. J.; Perez-Sanchez, H.; Puskas, I.; Roewer, N.; Forster, C.; Broscheit, J. A. Characterization, in vivo evaluation, and molecular modeling of different propofol−cyclodextrin complexes to assess their drug delivery potential at the blood−brain barrier level. *J. Chem. Inf. Model.* **2016**, *56*, 1914−1922.
(37) Satti, J. R.; Das, D. K.; Ray, D. Investigation of the thermal conductivity of propylene glycol nanofluids and comparison with correlations. *Int. J. Heat Mass Transfer* **2017**, *107*, 871−881.
(38) Liu, J.-H.; Gao, D.; He, L.-Q.; Moey, L. K.; Hua, K.; Liu, Z.-B. The phase diagram for the ternary system propylene glycol-sodium chloride-water and their application to platelet cryopreservation. *Zhong guo Shi Yan Xue Ye Xue Za Zhi* **2003**, *11*, 92−95.
(39) Malajczuk, C. J.; Hughes, Z. E.; Mancera, R. L. Molecular dynamics simulations of the interactions of DMSO, mono-and polyhydroxylated cryosolvents with a hydrated phospholipid bilayer. *Biochim. Biophys. Acta, Biomembr.* **2013**, *1828*, 2041−2055.
(40) Hughes, Z. E.; Malajczuk, C. J.; Mancera, R. L. The effects of cryosolvents on DOPC- β-sitosterol bilayers determined from molecular dynamics simulations. *J. Phys. Chem. B* **2013**, *117*, 3362−3375.
(41) Watkinson, R.; Guy, R.; Hadgraft, J.; Lane, M. Optimisation of cosolvent concentration for topical drug delivery−II: influence of propylene glycol on ibuprofen permeation. *Skin Pharmacol. Physiol.* **2009**, *22*, 225−230.
(42) Yamane, M.; Williams, A.; Barry, B. Terpene penetration enhancers in propylene glycol/water co-solvent systems: effectiveness and mechanism of action. *J. Pharm. Pharmacol.* **2011**, *47*, 978−989.
(43) Elsayed, M. M.; Abdallah, O. Y.; Naggar, V. F.; Khalafallah, N. M. PG-liposomes: novel lipid vesicles for skin delivery of drugs. *J. Pharm. Pharmacol.* **2010**, *59*, 1447−1450.
(44) Aye, M.; Di Giorgio, C.; De Mo, M.; Botta, A.; Perrin, J.; Courbiere, B. Assessment of the genotoxicity of three cryoprotectants used for human oocyte vitrification: dimethyl sulfoxide, ethylene glycol and propylene glycol. *Food Chem. Toxicol.* **2010**, *48*, 1905−1912.
(45) Andersen, F. Final report on the safety assessment of propylene-glycol and polypropylene glycols. *J. Am. Coll. Toxicol.* **1994**, *13*, 437−491.
(46) Center for the Evaluation of Risks to Human Reproduction and Others. NTP-CERHR Expert panel report on the reproductive and developmental toxicity of propylene glycol. *Reprod. Toxicol.* **2004**, *18*, 533−579.
(47) Sjostrom, J.; Mattsson, J.; Bergman, R.; Swenson, J. Hydrogen bond induced nonmonotonic composition behavior of the glass transition in aqueous binary mixtures. *J. Phys. Chem. B* **2011**, *115*, 10013−10017.
(48) Bednarska, D.; Koniorczyk, M. The influence of diol addition on water crystallization kinetics in mesopores. *J. Therm. Anal. Calorim.* **2019**, *138*, 2323−2337.
(49) Elamin, K.; Björklund, J.; Nyhlén, F.; Yttergren, M.; Mårtensson, L.; Swenson, J. Glass transition and relaxation dynamics of propylene glycol−water solutions confined in clay. *J. Chem. Phys.* **2014**, *141*, 034505.
(50) Cerveny, S.; Schwartz, G.; Alegria, A.; Bergman, R.; Swenson, J. Water dynamics in n-propylene glycol aqueous solutions. *J. Chem. Phys.* **2006**, *124*, 194501.
(51) Kearney, M.-C.; McKenna, P. E.; Quinn, H. L.; Courtenay, A. J.; Larrañeta, E.; Donnelly, R. F. Design and development of liquid drug reservoirs for microneedle delivery of poorly soluble drug molecules. *Pharmaceutics* **2019**, *11*, 605.
(52) Delgado, D. R.; Romdhani, A.; Martínez, F. Solubility of sulfamethizole in some propylene glycol+ water mixtures at several temperatures. *Fluid Phase Equil.* **2012**, *322*−*323*, 113−119.
(53) Vahdati, S.; Shayanfar, A.; Hanaee, J.; Martínez, F.; Acree, W. E., Jr; Jouyban, A. Solubility of carvedilol in ethanol+ propylene glycol mixtures at various temperatures. *Ind. Eng. Chem. Res.* **2013**, *52*, 16630−16636.
(54) Jiménez, D. M.; Cárdenas, Z. J.; Martínez, F. Solubility and apparent specific volume of some pharmaceutical salts in propylene glycol+ water mixtures at 298.15 K. *Chem. Eng. Commun.* **2016**, *203*, 1013−1019.
(55) Gao, Y.; Olsen, K. W. Molecular dynamics of drug crystal dissolution: simulation of acetaminophen form I in water. *Mol. Pharm.* **2013**, *10*, 905−917.
(56) Dwyer, C.; Viebke, C.; Meadows, J. Propofol induced micelle formation in aqueous block copolymer solutions. *Colloids Surf., A* **2005**, *254*, 23−30.
(57) Cho, J.; Cho, J. C.; Lee, P.; Lee, M.; Oh, E. Formulation and evaluation of an alternative triglyceride-free propofol microemulsion. *Arch Pharm. Res.* **2010**, *33*, 1375−1387.
(58) Momot, K. I.; Kuchel, P. W.; Chapman, B. E.; Deo, P.; Whittaker, D. NMR study of the association of propofol with nonionic surfactants. *Langmuir* **2003**, *19*, 2088−2095.
(59) Biswas, B.; Singh, P. C. The enhanced dissociation and associated surface structure of the anesthetic propofol at the water interface: vibrational sum frequency generation study. *Phys. Chem. Chem. Phys.* **2021**, *23*, 24646−24651.
(60) Tams, C.; Johnson, K. Prediction variability of combined pharmacokinetic pharmacodynamic models: a simulation study of propofol in combination with remifentanil and fentanyl. *J. Anesth. Clin. Res.* **2014**, *05*, 2.
(61) León, I.; Millán, J.; Castaño, F.; Fernández, J. A. A spectroscopic and computational study of propofol dimers and their hydrated clusters. *ChemPhysChem* **2012**, *13*, 3819−3826.
(62) Wang, H. J.; Kleinhammes, A.; Tang, P.; Xu, Y.; Wu, Y. Critical role of water in the binding of volatile anesthetics to proteins. *J. Phys. Chem. B* **2013**, *117*, 12007−12012.
(63) LeBard, D. N.; Henin, J.; Eckenhoff, R. G.; Klein, M. L.; Brannigan, G. General Anesthetics Predicted to Block the GLIC Pore with Micromolar Affinity. *PLoS Comput. Biol.* **2012**, *8*, No. e1002532.
(64) Henin, J.; Brannigan, G.; Dailey, W. P.; Eckenhoff, R.; Klein, M. L. An atomistic model for simulations of the general anesthetic isoflurane. *J. Phys. Chem. B* **2010**, *114*, 604−612.
(65) Liu, L. T.; Willenbring, D.; Xu, Y.; Tang, P. General anesthetic binding to neuronal $\alpha_4\beta_2$ nicotinic acetylcholine receptor and its effect on global dynamics. *J. Phys. Chem. B* **2009**, *113*, 12581−12589.
(66) Arcario, M. J.; Mayne, C. G.; Tajkhorshid, E. Atomistic models of general anesthetics for use in in silico biological studies. *J. Phys. Chem. B* **2014**, *118*, 12075−12086.

https://doi.org/10.1021/acs.jpcb.3c04932
J. Phys. Chem. B XXXX, XXX, XXX−XXX

(67) Koubi, L.; Tarek, M.; Bandyopadhyay, S.; Klein, M. L.; Scharf, D. Membrane structural perturbations caused by anesthetics and nonimmobilizers: A molecular dynamics investigation. *Biophys. J.* **2001**, *81*, 3339−3345.
(68) Faulkner, C.; Santos-Carballal, D.; Plant, D. F.; de Leeuw, N. H. Atomistic molecular dynamics simulations of propofol and fentanyl in phosphatidylcholine lipid bilayers. *ACS Omega* **2020**, *5*, 14340−14353.
(69) Hansen, A. H.; Sørensen, K. T.; Mathieu, R.; Serer, A.; Duelund, L.; Khandelia, H.; Hansen, P. L.; Simonsen, A. C. Propofol modulates the lipid phase transition and localizes near the headgroup of membranes. *Chem. Phys. Lipids* **2013**, *175*−*176*, 84−91.
(70) Miguel, V.; Villarreal, M. A.; García, D. A. Effects of gabergic phenols on the dynamic and structure of lipid bilayers: A molecular dynamic simulation approach. *PLoS One* **2019**, *14*, No. e0218042.
(71) Ahmad, S.; Johnston, B. F.; Mackay, S. P.; Schatzlein, A. G.; Gellert, P.; Sengupta, D.; Uchegbu, I. F. In silico modelling of drug−polymer interactions for pharmaceutical formulations. *J. R. Soc. Interface* **2010**, *7*, S423−S433.
(72) Gutierrez, A.; Atilhan, M.; Aparicio, S. Theoretical study on deep eutectic solvents as vehicles for the delivery of anesthetics. *J. Phys. Chem. B* **2020**, *124*, 1794−1805.
(73) Van Der Spoel, D.; Lindahl, E.; Hess, B.; Groenhof, G.; Mark, A. E.; Berendsen, H. J. GROMACS: fast, flexible, and free. *J. Comput. Chem.* **2005**, *26*, 1701−1718.
(74) Abraham, M. J.; Murtola, T.; Schulz, R.; Páll, S.; Smith, J. C.; Hess, B.; Lindahl, E. GROMACS: High performance molecular simulations through multi-level parallelism from laptops to supercomputers. *SoftwareX* **2015**, *1*−*2*, 19−25.
(75) Vanommeslaeghe, K., Jr; MacKerell, A. D. Automation of the CHARMM General Force Field (CGenFF) I: bond perception and atom typing. *J. Chem. Inf. Model.* **2012**, *52*, 3144−3154.
(76) Vanommeslaeghe, K.; Hatcher, E.; Acharya, C.; Kundu, S.; Zhong, S.; Shim, J.; Darian, E.; Guvench, O.; Lopes, P.; Vorobyov, I.; et al. CHARMM general force field: A force field for drug-like molecules compatible with the CHARMM all-atom additive biological force fields. *J. Comput. Chem.* **2010**, *31*, 671−690.
(77) Price, D. J.; Brooks, C. L., III A modified TIP3P water potential for simulation with Ewald summation. *J. Chem. Phys.* **2004**, *121*, 10096−10103.
(78) Hess, B.; Bekker, H.; Berendsen, H. J. C.; Fraaije, J. G. E. M. LINCS: A linear constraint solver for molecular simulations. *J. Comput. Chem.* **1997**, *18*, 1463−1472.
(79) Essmann, U.; Perera, L.; Berkowitz, M. L.; Darden, T.; Lee, H.; Pedersen, L. G. A smooth particle mesh Ewald method. *J. Chem. Phys.* **1995**, *103*, 8577−8593.
(80) Darden, T.; York, D.; Pedersen, L. Particle mesh Ewald: An N log (N) method for Ewald sums in large systems. *J. Chem. Phys.* **1993**, *98*, 10089−10092.
(81) Bussi, G.; Donadio, D.; Parrinello, M. Canonical sampling through velocity rescaling. *J. Chem. Phys.* **2007**, *126*, 014101.
(82) Bussi, G.; Zykova-Timan, T.; Parrinello, M. Isothermal-isobaric molecular dynamics using stochastic velocity rescaling. *J. Chem. Phys.* **2009**, *130*, 074101.
(83) Parrinello, M.; Rahman, A. Polymorphic transitions in single crystals: A new molecular dynamics method. *J. Appl. Phys.* **1981**, *52*, 7182−7190.
(84) Nosé, S.; Klein, M. Constant pressure molecular dynamics for molecular systems. *Mol. Phys.* **1983**, *50*, 1055−1076.
(85) Humphrey, W.; Dalke, A.; Schulten, K. VMD: visual molecular dynamics. *J. Mol. Graph.* **1996**, *14* (1), 33−38.
(86) Rhys, N. H.; Gillams, R. J.; Collins, L. E.; Callear, S. K.; Lawrence, M. J.; McLain, S. E. On the structure of an aqueous propylene glycol solution. *J. Chem. Phys.* **2016**, *145*, 224504.
(87) Ferreira, E. S.; Voroshylova, I. V.; Koverga, V. A.; Pereira, C. M.; Cordeiro, M. N. D. New force field model for propylene glycol: insight to local structure and dynamics. *J. Phys. Chem. B* **2017**, *121*, 10906−10921.
(88) Gilani, A. G.; Dafrazi, A. A.; Delcheh, S. R.; Verpoort, F. Cyclopentanone−Alkanediol Systems: Experimental and Theoretical Study on Hydrogen-Bond Complex Formation. *Ind. Eng. Chem. Res.* **2020**, *59*, 18318−18334.
(89) Chakraborty, S.; Kumar, H.; Dasgupta, C.; Maiti, P. K. Confined water: structure, dynamics, and thermodynamics. *Accounts Chem. Res.* **2017**, *50*, 2139−2146.
(90) Allen, M. P.; Tildesley, D. *Computer Simulation of Liquids*; Oxford University Press, 1987.
(91) Ozkanlar, A. Structure of the Hydrogen-Bond Network in Binary Mixtures of Formamide and Methanol. *J. Solution Chem.* **2021**, *50*, 257−276.
(92) Zhang, N.; Li, W.; Chen, C.; Zuo, J. Molecular dynamics simulation of aggregation in dimethyl sulfoxide−water binary mixture. *Comput. Theor. Chem.* **2013**, *1017*, 126−135.
(93) McLain, S. E.; Soper, A. K.; Luzar, A. Investigations on the structure of dimethyl sulfoxide and acetone in aqueous solution. *J. Chem. Phys.* **2007**, *127*, 174515.
(94) Egorov, A. V.; Lyubartsev, A. P.; Laaksonen, A. Molecular dynamics simulation study of glycerol−water liquid mixtures. *J. Phys. Chem. B* **2011**, *115*, 14572−14581.
(95) Paul, W. B. In *Molecular dynamics simulation, elementary methods*; Haile, J. M., Ed.; Wiley: Chichester, 1992, p 489. hardcover,£ 47.50, ISBN 0-471-81966-2, 1993.
(96) Henao, A.; Salazar-Rios, J. M.; Guardia, E.; Pardo, L. C. Structure and dynamics of water plastic crystals from computer simulations. *J. Chem. Phys.* **2021**, *154*, 104501.
(97) Luzar, A.; Chandler, D. Structure and hydrogen bond dynamics of water−dimethyl sulfoxide mixtures by computer simulations. *J. Chem. Phys.* **1993**, *98*, 8160−8173.
(98) van der Spoel, D.; van Maaren, P. J.; Berendsen, H. J. C.; Berendsen, H. J. C. A systematic study of water models for molecular simulation: Derivation of water models optimized for use with a reaction field. *J. Chem. Phys.* **1998**, *108*, 10220−10230.
(99) Laage, D.; Hynes, J. T. On the molecular mechanism of water reorientation. *J. Phys. Chem. B* **2008**, *112*, 14230−14242.
(100) Kawasaki, T.; Kim, K. Spurious violation of the Stokes−Einstein−Debye relation in supercooled water. *Sci. Rep.* **2019**, *9*, 8118.
(101) Paesani, F.; Iuchi, S.; Voth, G. A. Quantum effects in liquid water from an ab initio-based polarizable force field. *J. Chem. Phys.* **2007**, *127*, 074506.
(102) Mallik, B. S.; Chandra, A. An ab initio molecular dynamics study of the frequency dependence of rotational motion in liquid water. *J. Mol. Liq.* **2008**, *143*, 31−34.
(103) Bandyopadhyay, S.; Chakraborty, S.; Bagchi, B. Secondary Structure Sensitivity of Hydrogen Bond Lifetime Dynamics in the Protein Hydration Layer. *J. Am. Chem. Soc.* **2005**, *127*, 16660−16667.
(104) Luzar, A.; Chandler, D. Effect of Environment on Hydrogen Bond Dynamics in Liquid Water. *Phys. Rev. Lett.* **1996**, *76*, 928−931.
(105) Chowdhary, J.; Ladanyi, B. M. Hydrogen Bond Dynamics at the Water/Hydrocarbon Interface. *J. Phys. Chem. B* **2009**, *113*, 4045−4053.
(106) Stillinger, F. H.; Rahman, A. Improved simulation of liquid water by molecular dynamics. *J. Chem. Phys.* **1974**, *60*, 1545−1557.
(107) Rapaport, D. C. Hydrogen bonds in water. *Mol. Phys.* **1983**, *50*, 1151−1162.
(108) Luzar, A. Resolving the hydrogen bond dynamics conundrum. *J. Chem. Phys.* **2000**, *113*, 10663−10675.

https://doi.org/10.1021/acs.jpcb.3c04932
J. Phys. Chem. B XXXX, XXX, XXX−XXX